Unfolded protein response signaling promotes myeloid cell production and cooperates with oncogenic mutation

Hyunjoo Choi[1], Sang-Eun Jung[1], Hyojung Paik[2], Yesenia Earth[1], Jiye Yi[1], Maggie J. Cox[1], Stephen T. Oh[1] and Yoon-A Kang[1*]

[1] Division of Hematology, Department of Medicine, School of Medicine, Washington University in St. Louis, St. Louis, MO 63110, USA

[2] Center for Biomedical computing, Division of National Supercomputing R&D, Korea Institute of Science and Technology Information (KISTI), and University of Science and Technology (UST), Daejeon 34141, South Korea

[*] Corresponding author: Yoon-A Kang, PhD, Assistant Professor of Medicine, Washington University School of Medicine, 660 South Euclid Avenue, St Louis, MO 63110, USA. Phone: (314) 273-5954; Email: yoonakang@wustl.edu

Summary

Unfolded protein response (UPR) is an evolutionally conserved adaptive mechanism that promotes protein homeostasis under endoplasmic reticulum (ER) stress. UPR signaling has numerous functions in metabolism, cancer, immunology, and neurodegenerative diseases. Recent studies also showed that UPR signaling has important roles in hematopoietic stem and progenitor cell biology. However, whether UPR signaling regulates hematopoietic lineage fate decision remains elusive. Here, we found that FcγR$^-$ MPP3 generates erythroid lineage and *Jak2*^{V617F} mutation leads to overproduction of erythroid cells by expanding FcγR$^-$ MPP3. We showed that UPR signaling increases myeloid cell production through promoting FcγR$^-$ MPP3 transition to granulocyte/macrophage progenitor (GMP) producing FcγR$^+$ MPP3 at the expense of erythroid lineage via the XBP1 pathway. Under a disease condition, UPR signaling cooperates with *Jak2*^{V617F} mutation and exacerbates disease phenotype as increasing red blood cells in a mouse model of polycythemia vera (PV) through the ATF4 pathway. Activation of UPR signaling also increased myeloid output in healthy donor bone marrow MPP cells while skewing the output towards erythroid lineage in PV patient bone marrow MPP cells. Together, our results identify a novel function of UPR signaling in hematopoietic lineage specification and provide critical insights into targeting UPR signaling in hematological malignancies.

Keywords

Hematopoietic stem cell (HSC); multipotent progenitor (MPP); myelopoiesis; unfolded protein response; *Jak2*^{V617F}; erythropoiesis; polycythemia vera.

Highlights

- UPR signaling promotes myeloid cell production at the expense of erythroid lineage.
- UPR signaling collaborates with *Jak2*^{V617F} mutation and increases red blood cell production.

Introduction

Myelopoiesis is a dynamic process starting from hematopoietic stem cells (HSCs) and multipotent progenitor (MPP) populations that incorporates various environment cues and produces myeloid cells to adapt organismal needs[1]. Activation of HSCs and remodeling of MPP compartment such as expansion of myeloid-biased MPP2 and MPP3 and myeloid-reprogramming of lymphoid-biased MPP4 lead to granulocyte/macrophage progenitors (GMP) expansion followed by mature myeloid cell production[2-4]. In particular, secretory MPP3 subset, $ER^{high}/Fc\gamma R^{+}$ MPP3 expansion, which is triggered by high Wnt and low Notch activity, directly amplifies myelopoiesis by secreting pro-myeloid cytokines[5,6]. Pro-inflammatory cytokines like IL-6, IL-1, or TNFα also act on multiple steps during this process to boost myeloid cell production[2,4,7,8]. Given the significant contribution of MPP to blood production and the functional consequences of lineage priming at the MPP levels[9,10], what regulates the MPP compartment, especially the myeloid-biased MPP holds tremendous implications in controlling myelopoiesis.

Unfolded protein response (UPR) is a survival mechanism that cells take to resolve abnormal accumulation of unfolded or misfolded proteins. Aberrant UPR signaling has been implicated in various pathophysiology including inflammation, metabolic disease, neurodegenerative diseases, and cancer[11]. Recent studies also show diverse functions of UPR signaling beyond protein homeostasis[11]. In the hematopoietic system, UPR preserves HSC pool integrity under stress condition[12]. IRE1α–XBP1 axis maintains HSC self-renewal and protects hematopoietic stem and progenitor cells (HSPCs) from myeloid leukemogenesis[13,14]. XBP1 controls cytokine secretion in macrophages, B cell differentiation, dendritic cell development, and platelet aggregation[15-19]. ATF4 deficiency reduces functional HSC number in the fetal liver and, in adult mice, impairs HSC function as well as causes erythroid differentiation defects[20-23]. Although UPR regulates many aspects of hematopoiesis, whether UPR signaling controls lineage fate decision in HSPCs is poorly understood. Here, we report that UPR signaling promotes myeloid production

at the cost of erythroid lineage and potentiates the pathophysiology of *Jak2*^{V617F} mutation under a disease condition, identifying the new regulatory function of UPR signaling in hematopoiesis.

Results

FcγR$^-$ MPP3 is an erythroid-primed population

We previously showed that multipotent progenitor 3 (MPP3) is composed of two distinct subsets[5]. Myeloid-primed secretory ER^{high}/FcγR$^+$ MPP3 (hereafter FcγR$^+$ MPP3; Lin$^-$/Sca-1$^+$/c-Kit$^+$/Flk2$^-$/CD150$^-$/CD48$^+$/FcγR$^+$) is a transitional population toward granulocyte/macrophage progenitor (GMP) commitment, while ER^{low}/FcγR$^-$ MPP3 (hereafter FcγR$^-$ MPP3; Lin$^-$/Sca-1$^+$/c-Kit$^+$/Flk2$^-$/CD150$^-$/CD48$^+$/FcγR$^-$) represents the true multipotent part of the MPP3 compartment capable of generating FcγR$^+$ MPP3 and differentiating towards other myeloid lineage fates like erythroid lineage[5]. We also showed that FcγR$^+$ MPP3 are specifically expanded in *BCR-ABL* driven chronic myeloid leukemia (CML) mouse model, where granulocyte overproduction is a defining hallmark of disease[5], reflecting the lineage potential of FcγR$^+$ MPP3. Interestingly, we found that MPP3 expansion was driven by FcγR$^-$ MPP3 in Jak2 mutant mouse model of polycythemia vera (PV) (*Jak2^{V617F}*), which is characterized by overproduction of erythrocytes (Figures 1A and S1A-C), indicating that increased FcγR$^-$ MPP3 drives megakaryocyte/erythroid progenitor (MEP) expansion and excessive production of erythroid cells. This data, together with specific expansion of FcγR$^+$ MPP3 in CML mouse models[5], show that MPP3 subsets are differentially expanded in different myeloproliferative neoplasm (MPN) mouse models based on the affected mature myeloid cells, mirroring the lineage potential of each MPP3 subset. To test whether Jak2 mutation augments erythroid lineage potential of FcγR$^-$ MPP3, we performed myeloid colony forming assays using FcγR$^-$ MPP3 isolated from littermate control and *Jak2^{V617F}* mice. FcγR$^-$ MPP3 from *Jak2^{V617F}* mice did not show enhanced erythroid colony forming capacity (Figure 1B). Similarly, short-term *in vivo* differentiation assays showed that *Jak2^{V617F}* FcγR$^-$ MPP3 have a comparable level of MEP production (Figure 1C), indicating that *Jak2^{V617F}* does not increase erythroid potential of FcγR$^-$ MPP3 per se. Rather,

Jak2^{V617F} increases erythroid-primed FcγR$^-$ MPP3 cell number, which results in erythroid overproduction. These data align with the previous study showing that *BCR-ABL* increases granulocyte production by expanding FcγR$^+$ MPP3 population, not through enhancing intrinsic granulocyte potential of FcγR$^+$ MPP3[5,6]. *Jak2*^{V617F} also did not change the lineage potential of other MPP subsets (Figure S1D). In contrast, *Jak2*^{V617F} HSCs had significantly increased erythroid colony formation, indicating that *Jak2*^{V617F} mutation confers HSCs to promote erythroid production via the increase of FcγR$^-$ MPP3 and MPP2 number (Figure S1D). To investigate whether *Jak2*^{V617F} differentially affects HSCs and FcγR$^-$ MPP3, we performed bulk RNA-sequencing (RNA-seq) using HSCs and FcγR$^-$ MPP3 isolated from control and *Jak2*^{V617F} mice. Principal component analysis (PCA) showed the clear segregation between control and *Jak2*^{V617F} harboring cells (Figure 1D). Interestingly, only 20% of the top 500 differentially expressed genes (DEGs) overlapped between HSCs and FcγR$^-$ MPP3 (Figure S1E). Indeed, KEGG pathway analysis on FcγR$^-$ MPP3 DEGs uniquely showed alterations in metabolic pathway, indicating that *Jak2*^{V617F} exerts distinct molecular effects in HSCs versus FcγR$^-$ MPP3 although cell cycle and DNA replication genes were commonly changed (Figures 1E and S1F). Altogether, our data demonstrate that FcγR$^-$ MPP3 leads to erythroid production and *Jak2*^{V617F} drives HSCs to overproduce FcγR$^-$ MPP3 and MPP2, which results in erythroid overproduction in a PV mouse model. These data also highlight the divided labor of MPP3 subsets in producing different myeloid lineage cells.

UPR signaling promotes myelopoiesis at the cost of erythropoiesis

Considering the hierarchy from FcγR$^-$ MPP3 to FcγR$^+$ MPP3[5], signaling that promotes this transition is likely critical in balancing erythroid versus granulocyte/macrophage (G/M) output. To identify such regulators, we scrutinized bulk RNA-seq data of FcγR$^-$ MPP3 and FcγR$^+$ MPP3[5]. UPR genes (e.g., *Edem1,*

Calr, Hspa1l, Ero1l, Rpn1, Xbp1) were enriched in FcγR$^+$ MPP3, whereas erythroid genes (e.g., *Hbb-b1, Gata2*) were enriched in FcγR$^-$ MPP3. XBP1, the key regulator of UPR, was predicted to inhibit erythroid fate choice[24]. We therefore tested whether UPR activation promotes FcγR$^-$ to FcγR$^+$ MPP3 transition using myeloid colony forming assays. Treatment of FcγR$^-$ MPP3 with UPR inducers tunicamycin (Tuni) and thapsigargin (Thap) significantly increased granulocyte and macrophage colony formation while decreasing erythroid colony (Figures 2A and S2A). To directly measure FcγR$^+$ MPP3 production, we conducted short-term *in vitro* differentiation assays as previously done[5]. Upon UPR induction, FcγR$^+$ MPP3 production increased in a time dependent manner (Figure 2B). To test whether increased UPR signaling enhances FcγR$^+$ MPP3 production *in vivo*, we injected a low dose of tunicamycin (100 ng/g) for 5 days and analyzed bone marrow (BM) populations and peripheral blood (PB). The injection caused a slight decrease in body weight (4-5%) and reduced total MPP3, LSK (Lin$^-$/Sca-1$^+$/c-Kit$^+$), and myeloid progenitor (MP) populations (Figures S2B and S2C). However, within MPP3, FcγR$^+$ MPP3 significantly increased (Figure 2C). GMP also significantly increased at the expense of MEP within MP followed by elevated PB myeloid cells (Figure 2C). Probably due to the longer lifespan of erythrocytes (45 to 50 days)[25,26] and absolute high number, we did not observe decreased erythrocytes in the PB right after tunicamycin injection. To test whether UPR promotes myeloid cell production at the cost of erythroid cells as suggested by reduced MEP, we followed up erythroid cells for an extended period (Figure 2D). We took five days on and off cycle for repeated tunicamycin treatment. Hematocrit (HCT), the percentage of red blood cells (RBCs) in the blood, showed significant decrease after one cycle and further decreased as tunicamycin injection repeated while white blood cell and platelet numbers were comparable (Figures 2D and S2D). Absolute RBC number also reduced upon UPR activation (Figure 2D). These results demonstrate that UPR signaling facilitates FcγR$^-$ to FcγR$^+$ MPP3 conversion, which enhances myeloid cell production at the expense of erythroid cells.

UPR signaling cooperates with *Jak2^{V617F}* mutation and increases erythroid production under a disease condition

To examine whether UPR signaling elicits similar effects under an erythroid-potentiating disease condition, we injected tunicamycin into primary *Jak2^{V617F}* and littermate control mice. LSK and MP populations were significantly decreased in littermate controls but remained unchanged in *Jak2^{V617F}* mice (Figure 3A). Although MPP3 proportion declined in both groups, FcγR^{+} MPP3 did not consistently increase in *Jak2^{V617F}* mice (Figures 3B, S3A and S3B). Instead, we observed variable responses by *Jak2^{V617F}* mice upon UPR activation, potentially reflecting differences in disease stage, UPR sensitivity, or microenvironmental factors. Interestingly, MEP showed a significant increase at the cost of GMP followed by a higher RBC count in PB, indicating that UPR signaling collaborates with *Jak2^{V617F}* mutation, augmenting phenotypes associated with disease (Figures 3C and 3D). Of note, PB myeloid cells were still elevated, suggesting that UPR signaling also acted downstream of GMP as promoting myeloid output (Figure S3C). This finding reveals that UPR signaling functions in multiple levels to enhance myelopoiesis. To corroborate these findings, we injected tunicamycin into transplanted *Jak2^{V617F}* mice 6 weeks post-induction. Similar to the primary *Jak2^{V617F}* mice, transplanted *Jak2^{V617F}* mice showed heterogeneous responses and FcγR^{+} MPP3 did not invariably increase although LSK number reduced (Figures S3D and S3E). MEP also increased with the loss of GMP, and PB myeloid cells were elevated, recapitulating the primary model (Figures S3F and S3G). These data suggest that UPR signaling collaborates with *Jak2^{V617F}* mutation and regulates disease phenotype in addition to augmenting myelopoiesis. They also indicate that UPR signaling operates at multiple levels of the hematopoietic hierarchy to boost myeloid output.

To assess human relevance, we treated normal and PV patient BM MPPs (CD34^{+}/CD38^{-}/CD45RA^{-}/CD90^{-}/CD49f^{-})[27] with tunicamycin (0.6 μg/ml for 12 hours)[12] and performed myeloid colony forming assays. UPR activation increased GM colony formation in normal MPPs without reducing colony forming

capacity (Figures 3E and 3F). PV patient MPPs, however, significantly increased erythroid output with slightly higher plating efficiency (Figures 3E and 3G). These data confirm that UPR signaling enhances myeloid output in normal hematopoiesis and reinforces the pathophysiology of *Jak2*^{V617F} mutation in disease condition.

Two distinct UPR pathways differentially regulate myeloid versus erythroid lineage production.

To identify the major UPR pathway that drives myeloid cell production and the potential mechanism underlying cooperative role of UPR signaling with *Jak2*^{V617F} mutation, we focused on two UPR regulators, XBP1 and ATF4 because our RNA-seq analysis revealed that *Xbp1* was enriched in G/M-committed FcγR^{+} MPP3, ATF6 induces *Xbp1* mRNA, and hematopoietic ATF4 deficient mice have erythroid defects [5,21,23,28]. We treated MPP3 cells with tunicamycin (1.2 μg/ml for 12 hr) or thapsigargin (0.05 μM for 6 hr) and measured spliced and unspliced *Xbp1* transcripts using qRT-PCR. Increased ratio of spliced *Xbp1* over unspliced form is regarded as an indication of XBP1 transcriptional activity[28]. The ratio of spliced *Xbp1* was increased in both tunicamycin and thapsigargin-treated MPP3 (Figure 4A). Importantly, tunicamycin treatment also induced *Xbp1* transcription (Figure 4A). For the ATF4 pathway, we performed immunofluorescence assays and quantified nuclear ATF4 levels. Tunicamycin treatment activated ATF4 pathway, while thapsigargin treatment did not in MPP3 cells (Figure 4B). These data showed that only XBP1 pathway was activated by both tunicamycin and thapsigargin treatment in MPP3 cells, indicating that XBP1 is involved in the G/M priming of MPP3 cells. We then directly tested whether increasing XBP1 activity promotes myeloid cell production using IXA4, a highly selective, non-toxic IRE1/XBP1s activator[29]. We performed myeloid colony forming assays using methylcellulose. Upon IXA4 treatment (10 μM for 12 hr), MPP3 significantly increased G/M colony formation, similar to thapsigargin treatment but without compromising overall colony forming capacity (Figure 4C). Short-term *in vitro* differentiation

assays also confirmed that IXA4 treatment significantly increased FcγR$^+$ MPP3 production from FcγR$^-$ MPP3 (Figure 4D). To examine the function of XBP1 pathway in FcγR$^+$ MPP3 production *in vivo*, we used *Xbp1* conditional knockout mice (*Xbp1*^{cKO}; *Mx1-Cre::Xbp1*$^{fl/fl}$) and performed BM population analysis 8 weeks post-induction. Although there were no major changes in HSPC population, FcγR$^+$ MPP3 specifically and significantly increased followed by GMP expansion (Figure S4A). This data showed that XBP1 pathway regulates FcγR$^+$ MPP3 production. The reason why FcγR$^+$ MPP3 increased instead of decreased upon *Xbp1* deletion could be due to the compensatory mechanisms, the complex nature of *Xbp1* regulatory network, or secondary effects caused by *Xbp1* deletion in pan-hematopoietic cells and/or some BM niche cells (i.e., mesenchymal stroma cells or endothelial cells)[30]. Taken together, these data demonstrate that UPR signaling promotes myelopoiesis through XBP1 pathway.

To investigate ATF4 activity in *Jak2*^{V617F} mice upon UPR activation, we performed ATF4 immunofluorescence assays using MPP3 cells isolated from vehicle versus tunicamycin treated littermate control and *Jak2*^{V617F} mice. Tunicamycin (100 ng/g) was injected for five consecutive days before MPP3 isolation. Similar to *in vitro* tunicamycin treatment, MPP3 cells from tunicamycin injected mice had significantly higher nuclear ATF4 levels in littermate controls (Figure 4E). In *Jak2*^{V617F} mice, nuclear ATF4 level was already significantly higher compared to littermate controls (Figure 4E). This data indicates that *Jak2*^{V617F} activates ATF4 pathway, which probably, in part, contributes to erythroid overproduction given that ATF4 promotes erythropoiesis through ribosome biogenesis[21]. Our molecular data also reflects this ATF4 activation in MPP3 cells (e.g., purine metabolism, carbon metabolism, citrate cycle, nucleotide metabolism) as ATF4 activates metabolic pathway genes such as genes in amino acid metabolism, nucleotide synthesis and carbon metabolism[31] (Figure 1E). Tunicamycin injection further increased ATF4 activity in *Jak2*^{V617F} mice, suggesting that ATF4 hyperactivation upon tunicamycin injection help *Jak2*^{V617F} even more overproduce erythroid cells (Figures 3D and 4E). Of note, littermate

control mice with tunicamycin injection also had high nuclear ATF4 level but they did not increase RBC production, indicating that ATF4 activation is not sufficient to promote erythropoiesis (Figures 3D and 4E). To directly test whether ATF4 activation in *Jak2*^{V617F} mice promotes erythropoiesis, we treated transplanted *Jak2*^{V617F} mice with ATF4 inhibitor ISRIB[32,33] (1mg/kg) for five days and measured RBC three days post injection (Figure 4F). ISRIB treated *Jak2*^{V617F} mice significantly decreased RBC number while maintaining other blood counts (Figures 4F and S4B). In primary *Jak2*^{V617F} mice, ISRIB injection also reduced RBC, but littermate control mice injected with ISRIB showed no difference in RBC number, indicating that ATF4 activation enhances erythroid production in collaboration with *Jak2*^{V617F} (Figure S4C). Altogether, these results show that two distinct UPR pathways differentially regulate myeloid versus erythroid lineage production whereby XBP1 controls myelopoiesis while ATF4 modulates erythropoiesis in a collaborative manner.

Discussion

Recent studies demonstrated that UPR signaling controls HSPC biology[12-14,20-22]. Whether UPR signaling regulates lineage fate decision in the hematopoietic system remains unclear. Considering UPR is elevated in many cancers and targeting UPR signaling is considered as therapeutic interventions[11], whether UPR signaling alters hematopoietic lineage output is an important consideration when targeting UPR in cancers. Here, we found that UPR signaling promotes myelopoiesis by increasing the transition of erythroid-primed FcγR$^-$ MPP3 to myeloid-committed FcγR$^+$ MPP3, which leads to GMP expansion followed by myeloid cell increase in PB through XBP1 pathway. These increased myeloid cells cost erythroid production, indicating that MPP3 is the divergent point of myeloid versus erythroid lineage specification. These data also suggest that UPR signaling controls myeloid versus erythroid output in the hematopoietic system. Especially, sustained UPR activation progressively decreased RBC level in the body, implying that prolonged up-regulation of UPR signaling itself can cause anemia in hematological malignancies.

In a mouse model of PV, UPR signaling cooperates with *Jak2*^{V617F} mutation and increases erythroid cells via ATF4 pathway. ATF4 was already activated in *Jak2*^{V617F} mice as evidenced by up-regulation of canonical ATF4 metabolic target genes (e.g., *Phgdh*, *Shmt1*, *Ass1*, *Psat1*, etc.) in *Jak2*^{V617F} FcγR$^-$ MPP3 and high nuclear ATF4 level in *Jak2*^{V617F} MPP3. Given that Jak2 signaling activates protein kinase R (PKR), a key eIF2α kinase, which, in turn, can activate ATF4 and that *Jak2*^{V617F} constitutively activates downstream signaling pathways leading to cellular proliferation[34,35], ATF4 activation in *Jak2*^{V617F} mice is not surprising. We showed that ATF4 exerts its effect on erythroid-primed FcγR$^-$ MPP3 and ATF4 hyperactivation further increases erythroid overproduction in *Jak2*^{V617F} mice. Lowering ATF4 activity in control mice did not decrease RBC number, reinforcing the idea that ATF4 activity itself is not sufficient

to increase erythropoiesis in steady state. How much ATF4 activity contributes to *Jak2*^{V617F} other phenotypes will be of interest to consider targeting ATF4 as a therapeutic intervention in PV.

Upon tunicamycin injection, some *Jak2*^{V617F} mice increased FcγR^{+} MPP3 but the others did not. This could be possibly because the tunicamycin dose we injected was not strong enough to overpower the driving force of *Jak2*^{V617F} mutation to erythroid lineage. Although MEP was relatively expanded at the expense of GMP in the MP compartment, the absolute number of GMP was not significantly reduced in *Jak2*^{V617F} mice. In addition, PB myeloid cells still significantly increased, indicating that myelopoiesis is not just a linear cascading process and that UPR signaling also acts on downstream of GMP to enhance myelopoiesis potentially through its canonical pro-survival function. The increase of PB myeloid cells also implies that *Jak2*^{V617F} may provide a self-enforcing feedback loop, which causes the progression of PV to more advanced diseases like myelofibrosis by constantly activating UPR signaling. Recent study revealed that type 2 calreticulin mutations activate ATF6 to enhance survival in MPN[36], providing another evidence that disease-causing mutation collaborates with UPR signaling for pathogenesis. Further investigation into whether UPR components interact with other hematologic/oncogenic mutations and their functional consequences will provide valuable therapeutic insights. Taken together, our study uncovers that distinct UPR pathways function in lineage-specific production in a context-dependent manner, wherein UPR signaling promotes myelopoiesis through the XBP1 pathway under normal conditions, while enhancing erythropoiesis via the ATF4 pathway in collaboration with *Jak2*^{V617F} mutation.

Limitations of the study

Myelopoiesis is a complex process starting from HSCs to remodeling of MPP compartments to downstream GMP cluster formation to mature myeloid cell production[1]. While we reported here the function of UPR pathway in myelopoiesis by promoting the conversion of erythroid-primed FcγR$^-$ MPP3 to G/M-committed FcγR$^+$ MPP3 via XBP1 pathway, the whole picture will be completed with the investigation of the role of UPR signaling in HSC lineage priming, myeloid reprogramming of lymphoid-biased MPP4, a well-known phenomenon during myeloid regeneration and myeloid leukemia, GMP cluster formation, and mature myeloid cell production downstream of GMP[2-4,6]. Similarly, while we focused on the function of erythroid-primed FcγR$^-$ MPP3 in erythroid production in *Jak2*^{V617F} mice, megakaryocyte-biased MPP2 can produce erythroid cells as good as MPP3[3]. The better understanding of MPP2 contribution to erythroid production and how UPR activation changes MPP2 biology in terms of their lineage output and molecular rewiring will provide more comprehensive strategies to target UPR signaling as therapeutic options.

Acknowledgements

We thank Dr. Link (Wash U) for *UBC-Cre* mice, Dr. Glimcher (Dana-Farber Cancer Institute) for *Xbp1*$^{fl/fl}$ mice, Lina Joo (Wash U) for technical assistance, and Dr. Sykes (Wash U) for critical advice for experimental design. This work was supported by NIH grant K01 DK120780, R56DK139218, Leukemia Research Foundation P22-05724, American Cancer Society IRG-21-133-64-01 and CAT-24-1377095-01-CAT, NCI Specialized Program of Research Excellence in Leukemia (SPORE) DRP-2203, the Alvin J. Siteman Cancer Center through The Foundation for Barnes-Jewish Hospital AW00014358 to Y-A. Kang and NIH grant R01HL134952 to S.T. Oh.

Authorship and conflict-of-interest statements

Contribution: H. Choi and Y-A. Kang designed the study; H. Choi, S.E. Jung, Y. Earth, J. Yi and Y-A. Kang performed experiments, collected and analyzed data; H. Paik performed all the bioinformatic analyses; M.J. Cox and S.T. Oh provided PV patient samples; S.T. Oh provided *Vav1-Cre::Jak2*^{V617F} mice; H. Choi and Y-A. Kang wrote the manuscript; H. Choi, S.E. Jung, S.T. Oh and Y-A. Kang edited the manuscript. All authors read and approved the manuscript.

Disclosure of Conflicts of Interest: H. Choi, S.E. Jung, Y. Earth, J. Yi, M. J. Cox, H. Paik, Y-A. Kang declare no competing financial interests. S.T. Oh has served as a consultant for Kartos Therapeutics, CTI BioPharma, Celgene–Bristol Myers Squibb, Disc Medicine, Blueprint Medicines, PharmaEssentia, Constellation, Geron, AbbVie, Sierra Oncology and Incyte.

Data Sharing Statement

Data are available upon request from the corresponding author, Yoon-A Kang (yoonakang@wustl.edu). RNA-seq data have been deposited in the Gene Expression Omnibus under accession code GSE297249.

Figure legends

Figure 1. FcγR$^-$ MPP3 expansion drives erythroid overproduction.

(A) Hematopoietic stem and progenitor cell (HSPC) and myeloid progenitor (MP) population analyses of littermate control (Ctrl) and *Mx1-Cre::Jak2*^{V617F} (*Jak2*^{V617F}) mice 12 weeks post-induction.

(B) Myeloid colony forming assays using FcγR$^-$ MPP3 isolated from littermate control and *Mx1-Cre::Jak2*^{V617F} mice 12 weeks post-induction (n = 8). Colony-forming units (CFUs) in methylcellulose assays were scored 8 days after plating. GEMM, granulocyte/erythroid/macrophage/megakaryocyte; GM, granulocyte/macrophage; G (or) M, granulocyte or macrophage; MegE, megakaryocyte/erythrocyte.

(C) Short-term *in vivo* differentiation assays. Donor cells were isolated from littermate control and *Mx1-Cre::Jak2*^{V617F} mice 12 weeks post induction (20,000 cells per mouse). Donor-derived cells were analyzed for MP (Lin$^-$/Sca-1$^-$/c-Kit$^+$) contributions at 3 days post-infusion. Representative FACS plots and quantification of donor-derived frequencies are shown.

(D) Principal component (PC) analysis of HSC and FcγR$^-$ MPP3 bulk RNA-seq data from littermate control and *Mx1-Cre::Jak2*^{V617F} mice. (E) KEGG pathway analysis of the top 500 differentially expressed genes (DEGs) in FcγR$^-$ MPP3 from littermate control and *Mx1-Cre::Jak2*^{V617F} mice. The DEG list is provided in Table S1.

Data are means ± S.D., and statistical significance was assessed by a two-tailed unpaired Student's *t-test*. * $p \leq 0.05$, ** $p \leq 0.01$, *** $p \leq 0.001$.

See also Figure S1.

Figure 2. UPR signaling promotes FcγR$^+$ MPP3 and myeloid lineage cell production at the expense of erythroid lineage.

(A) Myeloid colony forming assays using FcγR$^-$ MPP3 treated with tunicamycin (Tuni) for 16 hours (n = 8). Colony-forming units (CFUs) in methylcellulose assays were scored 6 days after plating. GEMM, granulocyte/erythroid/macrophage/megakaryocyte; GM, granulocyte/macrophage; G (or) M, granulocyte or macrophage; MegE, megakaryocyte/erythrocyte. Statistical significance is compared to control DMSO treatment.

(B) Short-term *in vitro* differentiation of FcγR$^-$ MPP3 upon tunicamycin (Tuni; 0.6 μg/ml) treatment. Cells (2,000 per well) were cultured for 6 or 12 hours (hr) with tunicamycin and cultured extra 24 or 18 hours, respectively, after washing out tunicamycin. Cells were then analyzed for HSPC markers. Representative FACS plots and quantification of FcγR$^+$ MPP3 production as fold change relative to control (Ctrl: DMSO treated FcγR$^-$ MPP3) are shown. The gray dotted line indicates the fold change of 1.

(C) Experimental scheme of *in vivo* tunicamycin injection and representative FACS plots showing the MPP3 and MP populations (left). Quantification of FcγR$^+$ MPP3, MP population, and PB myeloid cells (right) upon tunicamycin treatment. Tuni, tunicamycin; BM, bone marrow; PB, peripheral blood; MP, myeloid progenitor.

(D) Experimental scheme for repeated tunicamycin treatment in WT mice (left) and peripheral blood (PB) complete blood counts upon repeated tunicamycin treatment in WT mice (right) (n = 4-6). HCT, hematocrit; RBC, red blood cell; D, days.

Data are means ± S.D., and statistical significance was assessed by a two-tailed unpaired Student's *t-test*. * $p \leq 0.05$, ** $p \leq 0.01$, *** $p \leq 0.001$.

See also Figure S2.

Figure 3. UPR signaling increases erythroid production in *Jak2*^{V617F} mice.

(A) Experimental scheme (left) and changes in LSK (Lin^{-}/Sca-1^{+}/c-Kit^{+}) and myeloid progenitor (MP) populations in littermate control and *Jak2*^{V617F} mice upon tunicamycin treatment (right). Data represent the combined results from both *Vav1-Cre* and *Mx1-Cre* driven *Jak2*^{V617F} mice.

(B-D) Quantification of FcγR^{+} MPP3 (B), MP population (C), and PB red blood cell (RBC) count (D) upon tunicamycin injection. Data are means + S.D., and statistical significance was assessed by a two-tailed unpaired Student's *t-test*.

(E-G) Overall plating efficiency (E) and myeloid colony forming capacity of normal bone marrow (NBM) (F) and PV patient bone marrow (PV) (G) MPP cells upon tunicamycin treatment (n = 5). Human bone marrow MPP cells were treated with tunicamycin (0.6 μg/ml) for 12 hours and then plated onto the methylcellulose for myeloid colony forming assays. Colonies were counted after 14 days of culture. GEMM, granulocyte/erythroid/macrophage/megakaryocyte; GM, granulocyte or macrophage; E, burst-forming unit-erythroid (BFU-E) and colony-forming unit-erythroid (CFU-E); MK, megakaryocyte. Data are means - S.D., and statistical significance was assessed by a two-tailed paired Student's *t-test*.

Tuni, tunicamycin; BM, bone marrow; PB, peripheral blood; Ctrl, control. * $p \leq 0.05$, ** $p \leq 0.01$, *** $p \leq 0.001$.

See also Figure S3.

Figure 4. Two different UPR pathways function separately in distinct lineage production.

(A) Quantitative RT-PCR analyses of *Xbp1* transcripts upon tunicamycin (Tuni) (1.2 μg/ml for 12 hr) or thapsigargin (Thap) (0.05 μM for 6 hr) treatment. Xbp1s: spliced *Xbp1* transcript; Xbp1u: unspliced *Xbp1* transcript; Ratio: ratio of spliced over unspliced *Xbp1* transcript.

(B) Representative images and quantification of nuclear ATF4 positive MPP3 cells upon tunicamycin (1.2 μg/ml for 12 hr) or thapsigargin (0.05 μM for 6 hr) treatment. Scale bar: 10 μm.

(C) Quantification of myeloid colony formation upon IXA4 (10 μM) and thapsigargin (Thap; 0.05 μM) treatment for 12 hours (n = 4). CFU, colony forming unit; MegE, megakaryocyte/erythrocyte; G (or) M, granulocyte or macrophage; GM; granulocyte/macrophage, GEMM, granulocyte/erythroid/macrophage/megakaryocyte.

(D) Short-term *in vitro* differentiation of FcγR$^-$ MPP3 upon IXA4 treatment. Cells (2,000 per well) were cultured with IXA4 (10 μM) for 24 hours and then analyzed for HSPC markers. Representative FACS plots and quantification of FcγR$^+$ MPP3 production as fold change relative to control (Ctrl: DMSO treated FcγR$^-$ MPP3) are shown.

(E) Quantification of nuclear ATF4 positive MPP3 cells from vehicle versus tunicamycin treated control and *Jak2*^{V617F} mice.

(F) Experimental scheme and RBC count upon ISRIB injection in transplanted *Jak2*^{V617F} mice. Transplanted *Jak2*^{V617F} mice were prepared as shown in Figure S3D. Mice were injected with ISRIB (1mg/kg) 6 weeks post-induction. Statistical significance was assessed by a two-tailed paired Student's *t-test*.

Data are means ± S.D., and statistical significance was assessed by a two-tailed unpaired Student's t-test except for panel F. * $p \leq 0.05$; ** $p \leq 0.01$; *** $p \leq 0.001$.

See also Figure S4.

Figure S1. *Jak2*^{V617F} mutation differentially affects HSCs and FcγR$^-$ MPP3 population.

(A) Hematopoietic stem and progenitor cell (HSPC) and myeloid progenitor (MP) population analyses of littermate control (Ctrl) and *UBC-Cre::Jak2*^{V617F} (*Jak2*^{V617F}) mice 12 weeks post-induction.

(B-C) Red blood cell (RBC) counts upon *Jak2*^{V617F} induction in (B) *Mx1-Cre::Jak2*^{V617F} mice (n = 9 for control and 7 for *Jak2*^{V617F} up to 10 weeks and n = 19 for control and 22 for *Jak2*^{V617F} at 12 weeks) and (C) *UBC-Cre::Jak2*^{V617F} mice (n = 13 for control and 6 for *Jak2*^{V617F}). wks, weeks.

(D) Myeloid colony forming assays using HSC, MPP2, and MPP4 isolated from littermate control and *Mx1-Cre::Jak2*^{V617F} mice 12 weeks post-induction (n = 5). Colony-forming units (CFUs) in methylcellulose assays were scored 8 days after plating. GEMM, granulocyte/erythroid/macrophage/megakaryocyte; GM, granulocyte/macrophage; G (or) M, granulocyte or macrophage; MegE, megakaryocyte/erythrocyte.

(E) Venn diagram showing the overlap of differentially expressed genes (DEGs) between HSC and FcγR$^-$ MPP3 from the top 500 DEG list in each group.

(F) KEGG pathway analysis of DEGs in HSCs between littermate control and *Mx1-Cre::Jak2*^{V617F} bulk RNA-seq data. The top 500 DEG list is presented in Table S2.

Data are means ± S.D., and statistical significance was assessed by a two-tailed unpaired Student's *t-test*. * $p \leq 0.05$, ** $p \leq 0.01$, *** $p \leq 0.001$.

Figure S2. UPR signaling increases myeloid production.

(A) Myeloid colony forming assays using FcγR$^-$ MPP3 treated with thapsigargin (Thap) for 6 hours (n = 8). Colony-forming units (CFUs) in methylcellulose assays were scored 6 days after plating. GEMM, granulocyte/erythroid/macrophage/megakaryocyte; GM, granulocyte/macrophage; G (or) M, granulocyte or macrophage; MegE, megakaryocyte/erythrocyte. Statistical significance is compared to control DMSO treatment.

(B) Changes in LSK (Lin$^-$/Sca-1$^+$/c-Kit$^+$) and myeloid progenitor (MP) populations in wild type (WT) mice upon tunicamycin (Tuni) treatment.

(C) Quantification of hematopoietic stem and progenitor cell (HSPC) populations in wild type mice upon tunicamycin treatment. Results are expressed as a percentage of LSK.

(D) Peripheral blood (PB) complete blood counts upon repeated tunicamycin treatment in WT mice (n = 4-6). WBC, white blood cell; PLT, platelet.

Data are means ± S.D., and statistical significance was assessed by a two-tailed unpaired Student's *t-test*.

* $p \leq 0.05$, ** $p \leq 0.01$, *** $p \leq 0.001$.

Figure S3. UPR signaling acts at multiple levels of the hematopoietic hierarchy to promote myeloid cell production.

(A-B) Hematopoietic stem and progenitor cell (HSPC) population changes in littermate control (ctrl) (A) and *Jak2*^{V617F} mice (B) upon tunicamycin (Tuni) treatment. Results are expressed as a percentage of LSK.

(C) Quantification of peripheral blood (PB) myeloid cells upon tunicamycin treatment in littermate controls and *Jak2*^{V617F} mice.

(D) Experimental scheme (left) and LSK and MP population changes in transplanted *Jak2*^{V617F} mice upon tunicamycin treatment (right). One million bone marrow (BM) cells from *Mx1-Cre::Jak2*^{V617F} (*Jak2*^{V617F}) mice were transplanted into lethally irradiated WT recipient mice. Six weeks post-transplantation, 10 μg polyI:C was injected three times every other day to induce *Jak2*^{V617F} expression. After six-week induction, 100 ng/g tunicamycin was injected for five consecutive days, and BM populations and PB myeloid cells were analyzed. Trxpl, transplantation; WT, wild type; Tuni, tunicamycin.

(E-G) Changes in FcγR^{+} MPP3 (E), myeloid progenitor (MP) population (F), and PB myeloid cells (G) in transplanted *Jak2*^{V617F} mice upon tunicamycin injection.

Data are means + S.D., and statistical significance was assessed by a two-tailed unpaired Student's *t-test*.

* $p \leq 0.05$, ** $p \leq 0.01$, *** $p \leq 0.001$.

Figure S4. XBP1 controls myelopoiesis while ATF4 regulates erythroid cell production.

(A) Hematopoietic stem and progenitor cell (HSPC) and myeloid progenitor (MP) population analyses of littermate control (Ctrl) and *Mx1-Cre::Xbp1*$^{fl/fl}$ (*Xbp1*^{cKO}) mice 8 weeks post-deletion. Data are means + S.D., and statistical significance was assessed by a two-tailed unpaired Student's *t-test*.

(B) White blood cell (WBC) and platelet (PLT) count upon ISRIB injection in transplanted *Jak2*^{V617F} mice. Transplanted *Jak2*^{V617F} mice were prepared as shown in Figure S3D. Mice were injected with ISRIB (1mg/kg) 6 weeks post-induction.

(C) RBC count upon ISRIB injection (1mg/kg) in littermate control and *Jak2*^{V617F} mice. Both groups were injected with ISRIB. Injection scheme is shown in Figure 4F. Ctrl, littermate control mice.

Statistical significance was assessed by a two-tailed paired Student's *t-test* for panel B and C.

* $p \leq 0.05$, ** $p \leq 0.01$.

Tables

Supplementary Table 1. Top 500 differentially expressed gene (DEG) list between control and *Jak2*^{V617F} FcγR^{-} MPP3

Supplementary Table 2. Top 500 DEG list between control and *Jak2*^{V617F} HSCs

Supplementary Table 3. Patient sample information

References

1. Olson, O.C., Kang, Y.A., and Passegue, E. (2020). Normal Hematopoiesis Is a Balancing Act of Self-Renewal and Regeneration. Cold Spring Harb Perspect Med *10*. 10.1101/cshperspect.a035519.
2. Reynaud, D., Pietras, E., Barry-Holson, K., Mir, A., Binnewies, M., Jeanne, M., Sala-Torra, O., Radich, J.P., and Passegue, E. (2011). IL-6 controls leukemic multipotent progenitor cell fate and contributes to chronic myelogenous leukemia development. Cancer Cell *20*, 661-673. 10.1016/j.ccr.2011.10.012.
3. Pietras, E.M., Reynaud, D., Kang, Y.A., Carlin, D., Calero-Nieto, F.J., Leavitt, A.D., Stuart, J.M., Gottgens, B., and Passegue, E. (2015). Functionally Distinct Subsets of Lineage-Biased Multipotent Progenitors Control Blood Production in Normal and Regenerative Conditions. Cell Stem Cell *17*, 35-46. 10.1016/j.stem.2015.05.003.
4. Herault, A., Binnewies, M., Leong, S., Calero-Nieto, F.J., Zhang, S.Y., Kang, Y.A., Wang, X., Pietras, E.M., Chu, S.H., Barry-Holson, K., et al. (2017). Myeloid progenitor cluster formation drives emergency and leukaemic myelopoiesis. Nature *544*, 53-58. 10.1038/nature21693.
5. Kang, Y.A., Paik, H., Zhang, S.Y., Chen, J.J., Olson, O.C., Mitchell, C.A., Collins, A., Swann, J.W., Warr, M.R., Fan, R., and Passegue, E. (2023). Secretory MPP3 reinforce myeloid differentiation trajectory and amplify myeloid cell production. J Exp Med *220*. 10.1084/jem.20230088.
6. Kang, Y.A., Pietras, E.M., and Passegue, E. (2020). Deregulated Notch and Wnt signaling activates early-stage myeloid regeneration pathways in leukemia. J Exp Med *217*. 10.1084/jem.20190787.
7. Pietras, E.M., Mirantes-Barbeito, C., Fong, S., Loeffler, D., Kovtonyuk, L.V., Zhang, S., Lakshminarasimhan, R., Chin, C.P., Techner, J.M., Will, B., et al. (2016). Chronic interleukin-1 exposure drives haematopoietic stem cells towards precocious myeloid differentiation at the expense of self-renewal. Nat Cell Biol *18*, 607-618. 10.1038/ncb3346.
8. Yamashita, M., and Passegue, E. (2019). TNF-alpha Coordinates Hematopoietic Stem Cell Survival and Myeloid Regeneration. Cell Stem Cell *25*, 357-372 e357. 10.1016/j.stem.2019.05.019.
9. Rodriguez-Fraticelli, A.E., Wolock, S.L., Weinreb, C.S., Panero, R., Patel, S.H., Jankovic, M., Sun, J., Calogero, R.A., Klein, A.M., and Camargo, F.D. (2018). Clonal analysis of lineage fate in native haematopoiesis. Nature *553*, 212-216. 10.1038/nature25168.
10. Weinreb, C., Rodriguez-Fraticelli, A., Camargo, F.D., and Klein, A.M. (2020). Lineage tracing on transcriptional landscapes links state to fate during differentiation. Science *367*. 10.1126/science.aaw3381.
11. Hetz, C., Zhang, K., and Kaufman, R.J. (2020). Mechanisms, regulation and functions of the unfolded protein response. Nat Rev Mol Cell Biol *21*, 421-438. 10.1038/s41580-020-0250-z.
12. van Galen, P., Kreso, A., Mbong, N., Kent, D.G., Fitzmaurice, T., Chambers, J.E., Xie, S., Laurenti, E., Hermans, K., Eppert, K., et al. (2014). The unfolded protein response governs integrity of the haematopoietic stem-cell pool during stress. Nature *510*, 268-272. 10.1038/nature13228.
13. Liu, L., Zhao, M., Jin, X., Ney, G., Yang, K.B., Peng, F., Cao, J., Iwawaki, T., Del Valle, J., Chen, X., and Li, Q. (2019). Adaptive endoplasmic reticulum stress signalling via IRE1alpha-XBP1 preserves self-renewal of haematopoietic and pre-leukaemic stem cells. Nat Cell Biol *21*, 328-337. 10.1038/s41556-019-0285-6.
14. Barton, B.M., Son, F., Verma, A., Bal, S.K., Tang, Q., Wang, R., Umphred-Wilson, K., Khan, R., Trichka, J., Dong, H., et al. (2025). IRE1alpha-XBP1 safeguards hematopoietic stem and

progenitor cells by restricting pro-leukemogenic gene programs. Nat Immunol *26*, 200-214. 10.1038/s41590-024-02063-w.
15. Martinon, F., Chen, X., Lee, A.H., and Glimcher, L.H. (2010). TLR activation of the transcription factor XBP1 regulates innate immune responses in macrophages. Nat Immunol *11*, 411-418. 10.1038/ni.1857.
16. Iwakoshi, N.N., Lee, A.H., Vallabhajosyula, P., Otipoby, K.L., Rajewsky, K., and Glimcher, L.H. (2003). Plasma cell differentiation and the unfolded protein response intersect at the transcription factor XBP-1. Nat Immunol *4*, 321-329. 10.1038/ni907.
17. Zhang, K., Wong, H.N., Song, B., Miller, C.N., Scheuner, D., and Kaufman, R.J. (2005). The unfolded protein response sensor IRE1alpha is required at 2 distinct steps in B cell lymphopoiesis. J Clin Invest *115*, 268-281. 10.1172/JCI21848.
18. Iwakoshi, N.N., Pypaert, M., and Glimcher, L.H. (2007). The transcription factor XBP-1 is essential for the development and survival of dendritic cells. J Exp Med *204*, 2267-2275. 10.1084/jem.20070525.
19. Jain, K., Tyagi, T., Du, J., Hu, X., Patell, K., Martin, K.A., and Hwa, J. (2022). Unfolded Protein Response Differentially Modulates the Platelet Phenotype. Circ Res *131*, 290-307. 10.1161/CIRCRESAHA.121.320530.
20. Zhao, Y., Zhou, J., Liu, D., Dong, F., Cheng, H., Wang, W., Pang, Y., Wang, Y., Mu, X., Ni, Y., et al. (2015). ATF4 plays a pivotal role in the development of functional hematopoietic stem cells in mouse fetal liver. Blood *126*, 2383-2391. 10.1182/blood-2015-03-633354.
21. Zheng, Z., Yang, S., Gou, F., Tang, C., Zhang, Z., Gu, Q., Sun, G., Jiang, P., Wang, N., Zhao, X., et al. (2024). The ATF4-RPS19BP1 axis modulates ribosome biogenesis to promote erythropoiesis. Blood *144*, 742-756. 10.1182/blood.2023021901.
22. Sun, Y., Lin, X., Liu, B., Zhang, Y., Li, W., Zhang, S., He, F., Tian, H., Zhu, X., Liu, X., et al. (2021). Loss of ATF4 leads to functional aging-like attrition of adult hematopoietic stem cells. Sci Adv *7*, eabj6877. 10.1126/sciadv.abj6877.
23. Zhang, S., Macias-Garcia, A., Velazquez, J., Paltrinieri, E., Kaufman, R.J., and Chen, J.J. (2018). HRI coordinates translation by eIF2alphaP and mTORC1 to mitigate ineffective erythropoiesis in mice during iron deficiency. Blood *131*, 450-461. 10.1182/blood-2017-08-799908.
24. Tusi, B.K., Wolock, S.L., Weinreb, C., Hwang, Y., Hidalgo, D., Zilionis, R., Waisman, A., Huh, J.R., Klein, A.M., and Socolovsky, M. (2018). Population snapshots predict early haematopoietic and erythroid hierarchies. Nature *555*, 54-60. 10.1038/nature25741.
25. Dholakia, U., Bandyopadhyay, S., Hod, E.A., and Prestia, K.A. (2015). Determination of RBC Survival in C57BL/6 and C57BL/6-Tg(UBC-GFP) Mice. Comp Med *65*, 196-201.
26. Coupland, L.A., Cromer, D., Davenport, M.P., and Parish, C.R. (2010). A novel fluorescent-based assay reveals that thrombopoietin signaling and Bcl-X(L) influence, respectively, platelet and erythrocyte lifespans. Exp Hematol *38*, 453-461 e451. 10.1016/j.exphem.2010.03.003.
27. Notta, F., Zandi, S., Takayama, N., Dobson, S., Gan, O.I., Wilson, G., Kaufmann, K.B., McLeod, J., Laurenti, E., Dunant, C.F., et al. (2016). Distinct routes of lineage development reshape the human blood hierarchy across ontogeny. Science *351*, aab2116. 10.1126/science.aab2116.
28. Yoshida, H., Matsui, T., Yamamoto, A., Okada, T., and Mori, K. (2001). XBP1 mRNA is induced by ATF6 and spliced by IRE1 in response to ER stress to produce a highly active transcription factor. Cell *107*, 881-891. 10.1016/s0092-8674(01)00611-0.
29. Grandjean, J.M.D., Madhavan, A., Cech, L., Seguinot, B.O., Paxman, R.J., Smith, E., Scampavia, L., Powers, E.T., Cooley, C.B., Plate, L., et al. (2020). Pharmacologic IRE1/XBP1s activation

confers targeted ER proteostasis reprogramming. Nat Chem Biol *16*, 1052-1061. 10.1038/s41589-020-0584-z.

30. Velasco-Hernandez, T., Sawen, P., Bryder, D., and Cammenga, J. (2016). Potential Pitfalls of the Mx1-Cre System: Implications for Experimental Modeling of Normal and Malignant Hematopoiesis. Stem Cell Reports *7*, 11-18. 10.1016/j.stemcr.2016.06.002.
31. Wortel, I.M.N., van der Meer, L.T., Kilberg, M.S., and van Leeuwen, F.N. (2017). Surviving Stress: Modulation of ATF4-Mediated Stress Responses in Normal and Malignant Cells. Trends Endocrinol Metab *28*, 794-806. 10.1016/j.tem.2017.07.003.
32. Sidrauski, C., Acosta-Alvear, D., Khoutorsky, A., Vedantham, P., Hearn, B.R., Li, H., Gamache, K., Gallagher, C.M., Ang, K.K., Wilson, C., et al. (2013). Pharmacological brake-release of mRNA translation enhances cognitive memory. Elife *2*, e00498. 10.7554/eLife.00498.
33. Bao, J., Qian, Z., Liu, L., Hong, X., Che, H., and Wu, X. (2021). Pharmacological Disruption of Phosphorylated Eukaryotic Initiation Factor-2alpha/Activating Transcription Factor 4/Indian Hedgehog Protects Intervertebral Disc Degeneration via Reducing the Reactive Oxygen Species and Apoptosis of Nucleus Pulposus Cells. Front Cell Dev Biol *9*, 675486. 10.3389/fcell.2021.675486.
34. Bleiblo, F., Michael, P., Brabant, D., Ramana, C.V., Tai, T., Saleh, M., Parrillo, J.E., Kumar, A., and Kumar, A. (2013). JAK kinases are required for the bacterial RNA and poly I:C induced tyrosine phosphorylation of PKR. Int J Clin Exp Med *6*, 16-25.
35. Staerk, J., and Constantinescu, S.N. (2012). The JAK-STAT pathway and hematopoietic stem cells from the JAK2 V617F perspective. JAKSTAT *1*, 184-190. 10.4161/jkst.22071.
36. Arellano, N.S., Heaton, W.L., Nauman, M.C., Runnels, A.E., Gomez-Villa, J., Vanni, D., Gaviria, M., Fujita, M., Krah, N.M., Ciboddo, M., et al. (2025). Type 2 calreticulin mutations activate ATF6 to promote BCL-xL-mediated survival in myeloproliferative neoplasms. Blood *146*, 971-983. 10.1182/blood.2024026940.
37. Mullally, A., Lane, S.W., Ball, B., Megerdichian, C., Okabe, R., Al-Shahrour, F., Paktinat, M., Haydu, J.E., Housman, E., Lord, A.M., et al. (2010). Physiological Jak2V617F expression causes a lethal myeloproliferative neoplasm with differential effects on hematopoietic stem and progenitor cells. Cancer Cell *17*, 584-596. 10.1016/j.ccr.2010.05.015.
38. Hetz, C., Lee, A.H., Gonzalez-Romero, D., Thielen, P., Castilla, J., Soto, C., and Glimcher, L.H. (2008). Unfolded protein response transcription factor XBP-1 does not influence prion replication or pathogenesis. Proc Natl Acad Sci U S A *105*, 757-762. 10.1073/pnas.0711094105.
39. Kim, D., Paggi, J.M., Park, C., Bennett, C., and Salzberg, S.L. (2019). Graph-based genome alignment and genotyping with HISAT2 and HISAT-genotype. Nat Biotechnol *37*, 907-915. 10.1038/s41587-019-0201-4.
40. Patro, R., Duggal, G., Love, M.I., Irizarry, R.A., and Kingsford, C. (2017). Salmon provides fast and bias-aware quantification of transcript expression. Nat Methods *14*, 417-419. 10.1038/nmeth.4197.
41. Love, M.I., Huber, W., and Anders, S. (2014). Moderated estimation of fold change and dispersion for RNA-seq data with DESeq2. Genome Biol *15*, 550. 10.1186/s13059-014-0550-8.
42. Yu, G., Wang, L.G., Han, Y., and He, Q.Y. (2012). clusterProfiler: an R package for comparing biological themes among gene clusters. OMICS *16*, 284-287. 10.1089/omi.2011.0118.

STAR Methods

Contact for Reagent and Resource Sharing

Further information and requests for resources and reagents should be directed to and will be fulfilled by the Lead Contact, Yoon-A Kang, yoonakang@wustl.edu.

Experimental model and study participant details

Animals

All animal experiments were conducted at Washington University in accordance with IACUC protocols. CD45.2 C57BL/6J (000664), CD45.1 C57BL/6-BoyJ (002014) and B6.Cg-Tg(Mx1-cre)1Cgn/J (003556) mice were purchased from the Jackson Laboratory. Eight- to twelve-week-old CD45.2 C57BL/6J and CD45.1 C57BL/6-BoyJ were used. Cre driven Jak2^{V617F} knock-in mice[37] were used 12 weeks post-induction for *UBC*- and *Mx1-Cre* and when they reached at least 12 weeks old for *Vav-Cre*. *Mx1-Cre* driven Xbp1 floxed mice[38] were used 8 weeks post-deletion. Mx1-Cre was induced by injecting polyinosinic-polycytidylic acid (polyI:C; GE Healthcare, 27-4732-01) intraperitoneally (IP) at a dose of 10 mg/kg every other day for three times. UBC-Cre was induced by IP injection of 75 mg/kg tamoxifen (Sigma-Aldrich, T5648) once daily for five consecutive days. Respective wild type (WT) littermates or single transgenic animals were used as controls (Ctrl). Both male and female animals were used indifferently in the study.

Patient and healthy donor samples

Patient bone marrow samples were obtained according to a protocol approved by the Washington University Human Studies Committee (WU no. 01-1014). All patients previously provided consent to

have samples banked and were not newly recruited for this study. Healthy donor bone marrow samples were purchased from StemCell Technologies (70001) or Lonza (2M-125C). Patient sample list used in this study is provided in Supplementary Table 3.

Method details

Flow cytometry

Staining of hematopoietic cells was performed as previously described[5]. In brief, BM cells were obtained by crushing leg, arm, and pelvic bones in staining media composed of Hanks' buffered saline solution (HBSS) containing 2% heat-inactivated FBS (GenClone, 25-525H). Red blood cells (RBC) were removed by lysis with ACK (150 mM NH_4Cl/10 mM $KHCO_3$) buffer, and single-cell suspensions of BM cells were filtered through 40 μm Nylon mesh (Fisher Scientific 22-363-547) to get rid of dead cells after ACK treatment. Spleens were mechanically dissociated in staining media and ACK lysed to remove contaminating RBCs. Blood was collected in ACK buffer containing 10% EDTA from submandibular bleed and further lysed in ACK buffer to remove contaminating RBCs. Cellularity was determined by ViCELL-XR automated cell counter (Beckman-Coulter). For HSC and progenitor isolation, BM cells were pre-enriched for c-Kit+ cells using c-Kit microbeads (Miltenyi Biotec, 130-091-224) and an AutoMACS cell separator (Miltenyi Biotec). Unfractionated or c-Kit-enriched BM cells were then incubated with PE-Cy5 conjugated rat anti-mouse lineage antibodies (CD3, eBioscience, 15-0031-83; CD4, eBioscience, 15-0041-83; CD5, BioLegend, 100610; CD8, eBioscience, 15-0081-83; CD11b, eBioscience, 15-0112-83; B220, eBioscience, 15-0452-82; Gr1, eBioscience, 15-5931-83; Ter119, eBioscience, 15-5921-83), Sca-1-BV421 (BioLegend, 108128), c-Kit-APC-Cy7 (BioLegend, 105826), CD48-A647 (BioLegend, 103416), CD150-PE (BioLegend, 115904), and Flk2-Bio (eBioscience, 13-1351-85) followed by SA-BV605 (BioLegend, 405229), CD34-FITC (eBioscience, 11-0341-85) and

FcγR-PE-Cy7 (BioLegend, 101318). For short-term *in vitro* culture of FcγR$^-$ MPP3 with tunicamycin, cells were stained with Sca-1-BV421, c-Kit-APC-Cy7, CD48-A647, CD150-PE, and FcγR-PE-Cy7. For short-term *in vivo* differentiation assays, c-Kit-enriched recipient BM cells were stained with lineage cocktails as described above, CD45.1-PE (eBioscience, 12-0453-83), CD45.2-FITC (eBioscience, 11-0454-85), Sca-1-BV421, c-Kit-APC-Cy7, CD48-A647, CD150-PE, FcγR-PE-Cy7 and CD34-Bio (BioLegend, 119304) followed by SA-BV605 (BioLegend, 405229). Stained cells were finally re-suspended in staining media containing 1 µg/ml propidium iodide (PI) for dead cell exclusion. Cell isolations and analyses were performed on a FACS Aria III. Data collection was performed using FACSDiva (v9.4) and analysis was performed in FlowJo (v10.10, Treestar).

In vitro assays

All cultures were performed at 37°C in a 5% CO_2 water jacket incubator (Thermo Scientific) and all cytokines were purchased from PeproTech. For short-term *in vitro* differentiation of FcγR$^-$ MPP3, cells (2,000 per well of a 96-well plate) were grown in 200 µl base media consisting of Iscove's modified Dulbecco's media (IMDM) (Gibco) with 5% FBS (Gibco), 50 U/ml penicillin, 50 µg/ml streptomycin, 2 mM L-glutamine, 0.1 mM non-essential amino acids, 1 mM sodium pyruvate and 50 µM 2-mercaptoethanol, and containing SCF (25 ng/ml), TPO (25 ng/ml) and Flt3-L (25 ng/ml), IL-11 (25 ng/ml), IL-3 (10 ng/ml), GM-CSF (10 ng/ml) and EPO (4 U/ml) as cytokines. To activate UPR, cells were treated with either tunicamycin (Sigma, T7765) for 16 hours or thapsigargin (Sigma, T90330) for 6 hours and then plated onto the methylcellulose. For Xbp1 specific activation, cells were treated with 10 µM IXA4 (Selleck Chemicals, S9797) for 12 hours. For methylcellulose myeloid colony forming assays, 100 mouse cells were plated into 1ml methylcellulose (StemCell Technologies, M3231) supplemented with 50 U/ml penicillin, 50 µg/ml streptomycin, and the full cytokine cocktail described above as previously described[5].

Colonies were manually scored under a microscope after 6-8 days of culture. For human cells, 250 cells were cultured in StemSpan SFEM II media (StemCell Technologies, 09605) supplemented with StemSpan CD34+ expansion supplement (StemCell Technologies, 02691) and tunicamycin (0.6 μg/ml) for 12 hours and then plated onto 1ml methylcellulose (StemCell Technologies, M4034). Colonies were manually scored under a microscope after 14 days of culture. For short-term *in vitro* differentiation of FcγR$^-$ MPP3, cells were treated with 0.6 μg/ml tunicamycin for 6 or 12 hours and then cultured for extra 24 or 18 hours after washing out tunicamycin. For IXA4, cells were treated with 10 μM IXA4 for 24 hours before analysis.

In vivo assays

For short-term *in vivo* differentiation assays, 20,000 donor cells isolated from littermate control and *Mx1-Cre::Jak2*^{V617F} mice 12 weeks post-induction were retro-orbitally infused into recipient mice, which were analyzed for bone marrow (BM) contribution three days post infusion. Donor and recipient cells were identified by CD45.2-FITC and CD45.1-PE staining and recipient bone marrow cell population serves as an internal control for myeloid progenitor gating. For tunicamycin injection, mice were injected with tunicamycin (100 ng/g; IP) for five consecutive days before BM analysis. For repeated tunicamycin treatment, five consecutive day injection followed by five days off cycle was repeated. Tunicamycin was formulated in 1.5% DMSO (Sigma-Aldrich, D2650) and PBS. For ISRIB (MedChemExpress, HY-12495A) injection, mice were injected with ISRIB (1mg/kg; IP) for five consecutive days and then subjected to bleeding three days after last injection. ISRIB was formulated in 5% of DMSO, 60% of Kolliphor EL:ethanol (2:1 ratio), and 35% of saline. For transplantation experiments, recipient mice were lethally irradiated (10.5 Gy, delivered in split doses 4 hours apart) using an X-ray irradiator (Faxitron) and injected retro-orbitally with 1 x 10^6 BM cells. Transplanted mice were maintained on antibiotic-containing water for 4 weeks and analyzed for donor-derived chimerism by bleeding. Peripheral blood (PB) was

obtained from submandibular bleeding and collected in tubes containing 4 ml of ACK lysis buffer (150 mM NH_4Cl, 10 mM $KHCO_3$) supplemented with 10 mM EDTA for flow cytometry analyses. For CBC data, PB was obtained from submandibular bleeding and collected in Dipotassium EDTA tubes.

Gene expression analyses

For quantitative RT-PCR analyses, cells (5,000-8,000 cells/condition) were directly sorted into 500 µl Trizol LS (Life Technologies, 10296-010) and RNA was isolated using Direct-zol RNA Purification Kit (Zymo Research, R2060) according to the manufacturer's instructions, treated with DNase I (Invitrogen, 18068-015) and reverse-transcribed using SuperScript III kit and random hexamers (Invitrogen, 18080-051). Runs were performed on a QuantStudio 6 Pro (Applied Biosystems) using SYBR Green reagents (Kapa Biosystems, KK4603 or KK4620) and cDNA equivalent of 200 cells per reaction was used. Values were normalized to *Actb* expression levels and relative changes were calculated using the ΔΔCt method.

Immunofluorescence staining

For ATF4 staining, cells (2,000-3,000 cells/slide) were pipetted onto poly-L-lysine coated slides (Sigma-Aldrich, P0425), settled down for 15 min at room temperature (RT), fixed with 4% PFA for 10 min at RT, then washed 3 times with PBS, and permeabilized and blocked for 1 hour at RT with 0.1% Tween-20 in 10% FBS/PBS, which was then used as antibody incubation buffer for all the subsequent steps. Cells were then incubated overnight at 4 °C with a rabbit anti-mouse ATF4 (Cell Signaling, 11815S or Abcam, ab216839) primary antibody, washed 3 times with PBS, and incubated for 1 hour at RT with a goat anti-rabbit-A488 (Invitrogen, A32731) secondary antibody. After 3 time washing with PBS, slides were mounted with VectaShield Plus (Vector Laboratories, H-2000) containing 1 µg/ml DAPI. Cells were imaged on a Leica DM6 B Upright Microscopes (100x objective) using Leica Application Suite X

software (Leica Microsystems) and images were processed using Fiji (https://fiji.sc). For quantification, at least 100 cells per condition were randomly captured and ATF4 staining were scored by eye.

Bulk RNA-seq and bioinformatics analysis

RNA was isolated from 7,000 to 10,000 cells per sample using RNeasy Plus Micro Kit (Qiagen, 74034). RNA samples were submitted to the Genome Access Technology Center at the McDonnell Genome Institute for low input RNA sequencing. The initial quality control of raw reads was performed using FastQC (https://www.bioinformatics.babraham.ac.uk/projects/fastqc/), and HISAT2[39] assessed overall read coverage. The reference gene model of HISAT2 was based on the Mus musculus genome (GRCm38/mm10). The abundance of transcript reads was estimated using Salmon[40] and genes with low expressions were filtered out (<3 reads across compared set of samples). Differentially expressed gene (DEG) analysis was carried out using DEseq2[41] package of R. For the gene symbol annotations, we utilized MYGENE python package (https://pypi.org/project/mygene/). Normalized read counts were computed by dividing the raw read counts by size factors and fitting to a negative binomial distribution. P-values were first corrected by applying empirical estimation of the null distribution using the R package and then adjusted for multiple testing with the Benjamini–Hochberg correction. Genes with an adjusted P-value less than 0.05 and fold change values greater than 1.5 were considered as DEGs. The enrichment of gene signatures based on KEGG pathway was examined using R package clusterProfiler[42]. For gene set comparison between DEG sets, Venn diagrams were generated using matplotlib_venn package of python (https://pypi.org/project/matplotlib-venn/). For Principal component analysis (PCA), we utilized the plotPCA function of DESeq2 package of R. RNA-seq data have been deposited in the Gene Expression Omnibus under accession code GSE297249.

Statistical Analysis

All experiments were repeated as indicated. Data are expressed as mean + standard deviation or mean - standard deviation (S.D.). Mice for treatment and transplantation were randomized, samples were alternated whenever possible, and no blinding protocol was used. Statistical significance was evaluated by a two-tailed unpaired Student's t-test unless otherwise indicated. P values < 0.05 were considered statistically significant. Figures were made with GraphPad Prism (v10.6.1) and Adobe Illustrator (2025).

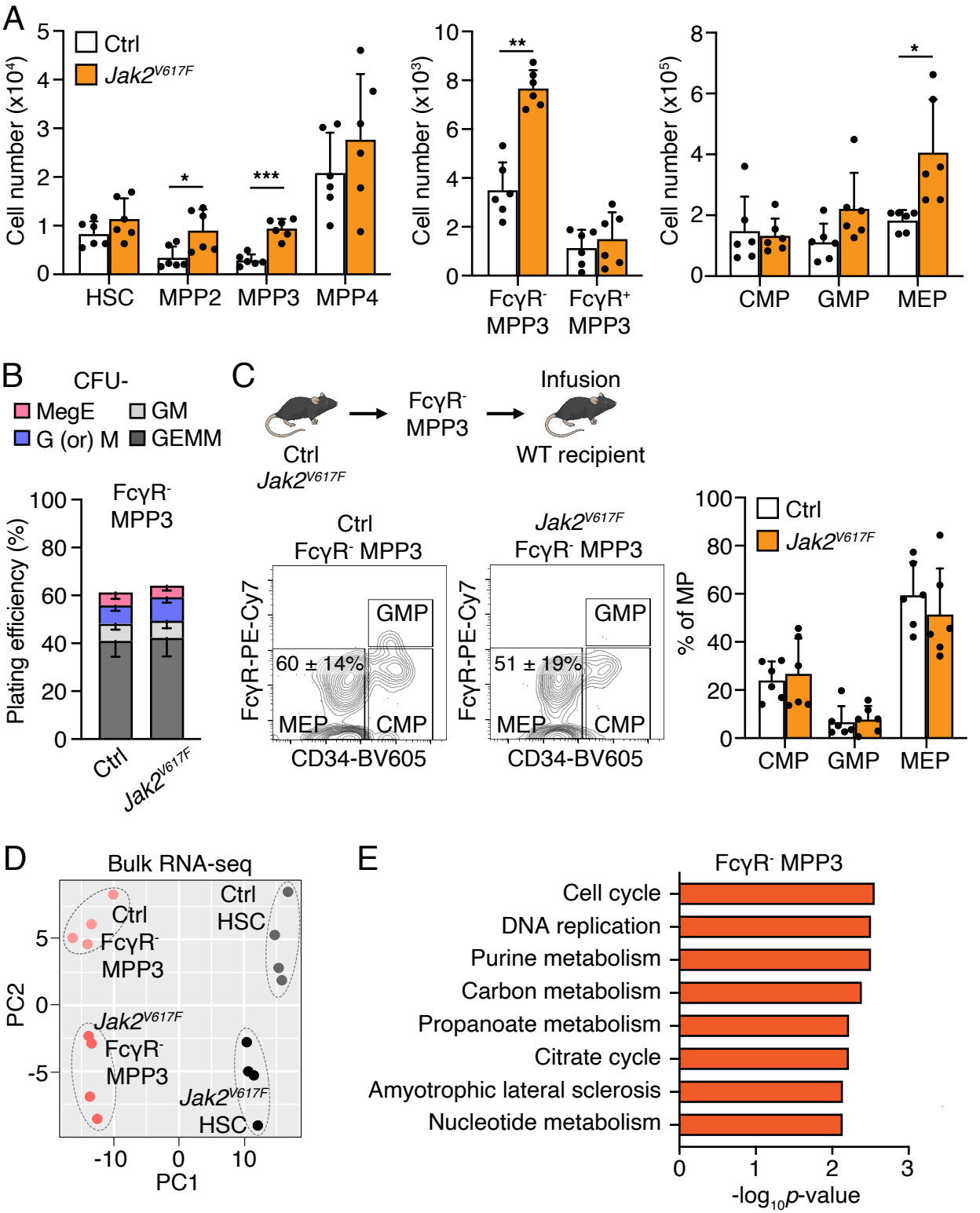
A
Ctrl
Jak2V617F
Cell number (x10^4)
HSC
MPP2
MPP3
MPP4
Cell number (x10^3)
FcγR- MPP3
FcγR+ MPP3
Cell number (x10^5)
CMP
GMP
MEP
B
CFU-
MegE
GM
G (or) M
GEMM
FcγR- MPP3
Plating efficiency (%)
Ctrl
Jak2V617F
C
Ctrl
Jak2V617F
FcγR- MPP3
Infusion
WT recipient
Ctrl
FcγR- MPP3
Jak2V617F
FcγR- MPP3
FcγR-PE-Cy7
CD34-BV605
GMP
MEP
CMP
60 ± 14%
51 ± 19%
% of MP
D
Bulk RNA-seq
Ctrl
FcγR- MPP3
Ctrl
HSC
Jak2V617F
FcγR- MPP3
Jak2V617F
HSC
PC2
PC1
E
FcγR- MPP3
Cell cycle
DNA replication
Purine metabolism
Carbon metabolism
Propanoate metabolism
Citrate cycle
Amyotrophic lateral sclerosis
Nucleotide metabolism
-log10p-value

Figure 1

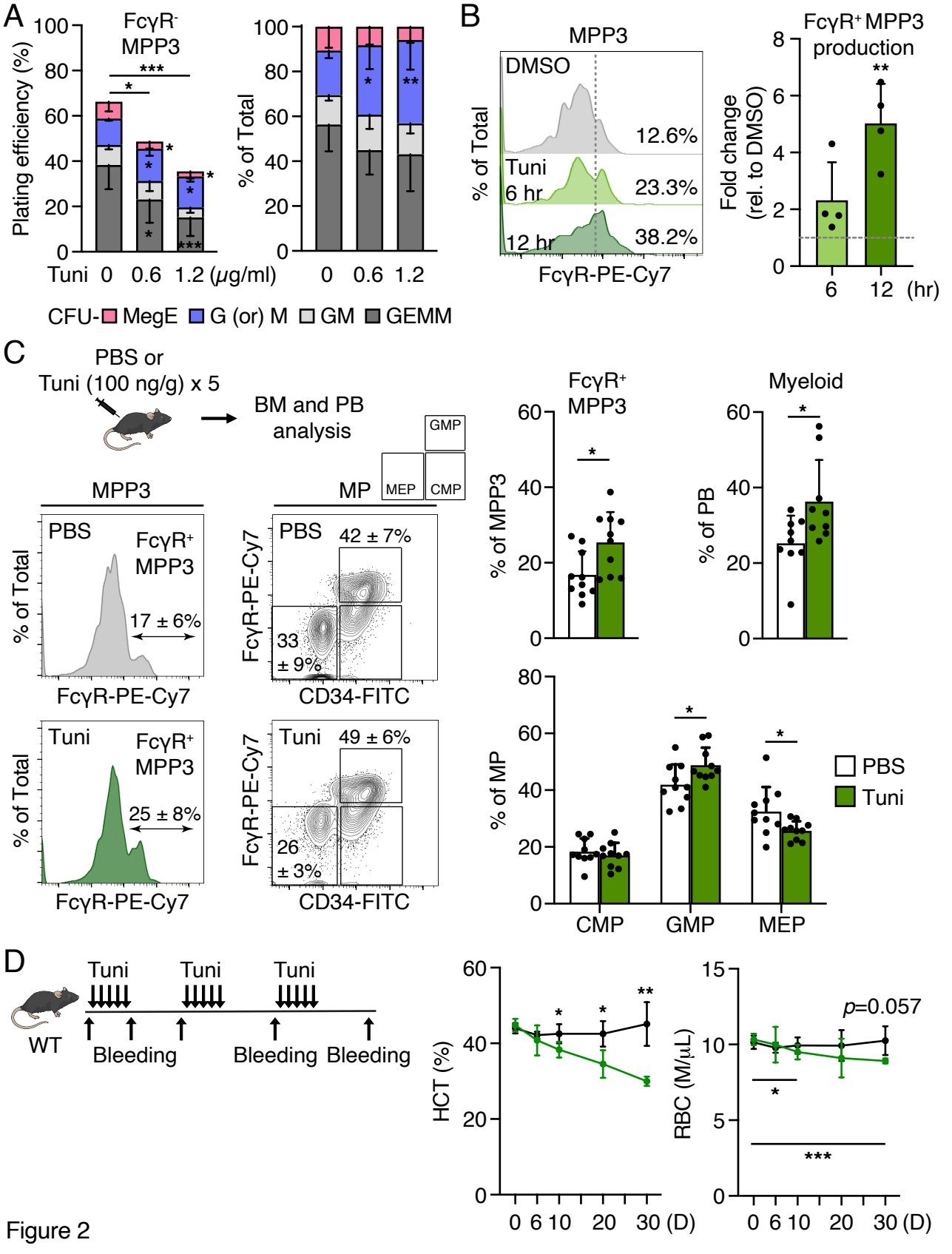
A
FcγR-
MPP3
Plating efficiency (%)
Tuni 0 0.6 1.2 (μg/ml)
% of Total
0 0.6 1.2
CFU- MegE G (or) M GM GEMM
B
MPP3
DMSO
12.6%
Tuni
6 hr
23.3%
12 hr
38.2%
% of Total
FcγR-PE-Cy7
FcγR+ MPP3
production
Fold change
(rel. to DMSO)
6 12 (hr)
C
PBS or
Tuni (100 ng/g) x 5
BM and PB
analysis
GMP
MEP
CMP
MPP3
MP
PBS
FcγR+
MPP3
17 ± 6%
42 ± 7%
33
± 9%
Tuni
25 ± 8%
49 ± 6%
26
± 3%
FcγR-PE-Cy7
CD34-FITC
FcγR+
MPP3
Myeloid
% of MPP3
% of PB
% of MP
PBS
Tuni
CMP GMP MEP
D
Tuni
WT
Bleeding
HCT (%)
RBC (M/μL)
p=0.057
0 6 10 20 30 (D)

Figure 2

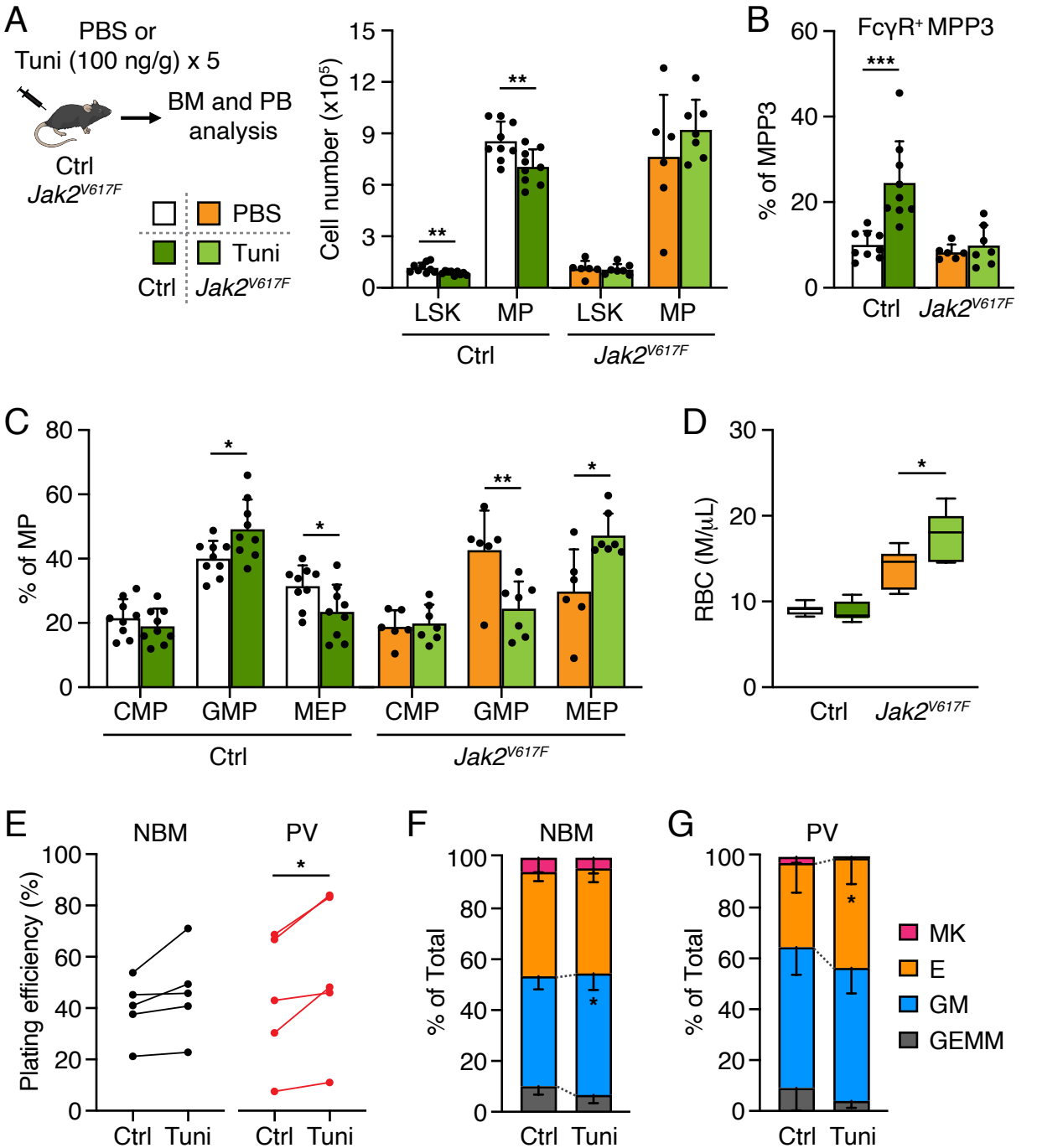
A
PBS or
Tuni (100 ng/g) x 5
BM and PB
analysis
Ctrl
Jak2V617F
PBS
Tuni
Ctrl
Jak2V617F
Cell number (x10^5)
LSK
MP
LSK
MP
Ctrl
Jak2V617F
B
FcγR+ MPP3
% of MPP3
Ctrl
Jak2V617F
C
% of MP
CMP
GMP
MEP
CMP
GMP
MEP
Ctrl
Jak2V617F
D
RBC (M/μL)
Ctrl
Jak2V617F
E
NBM
PV
Plating efficiency (%)
Ctrl
Tuni
Ctrl
Tuni
F
NBM
% of Total
Ctrl
Tuni
G
PV
% of Total
Ctrl
Tuni
MK
E
GM
GEMM

Figure 3

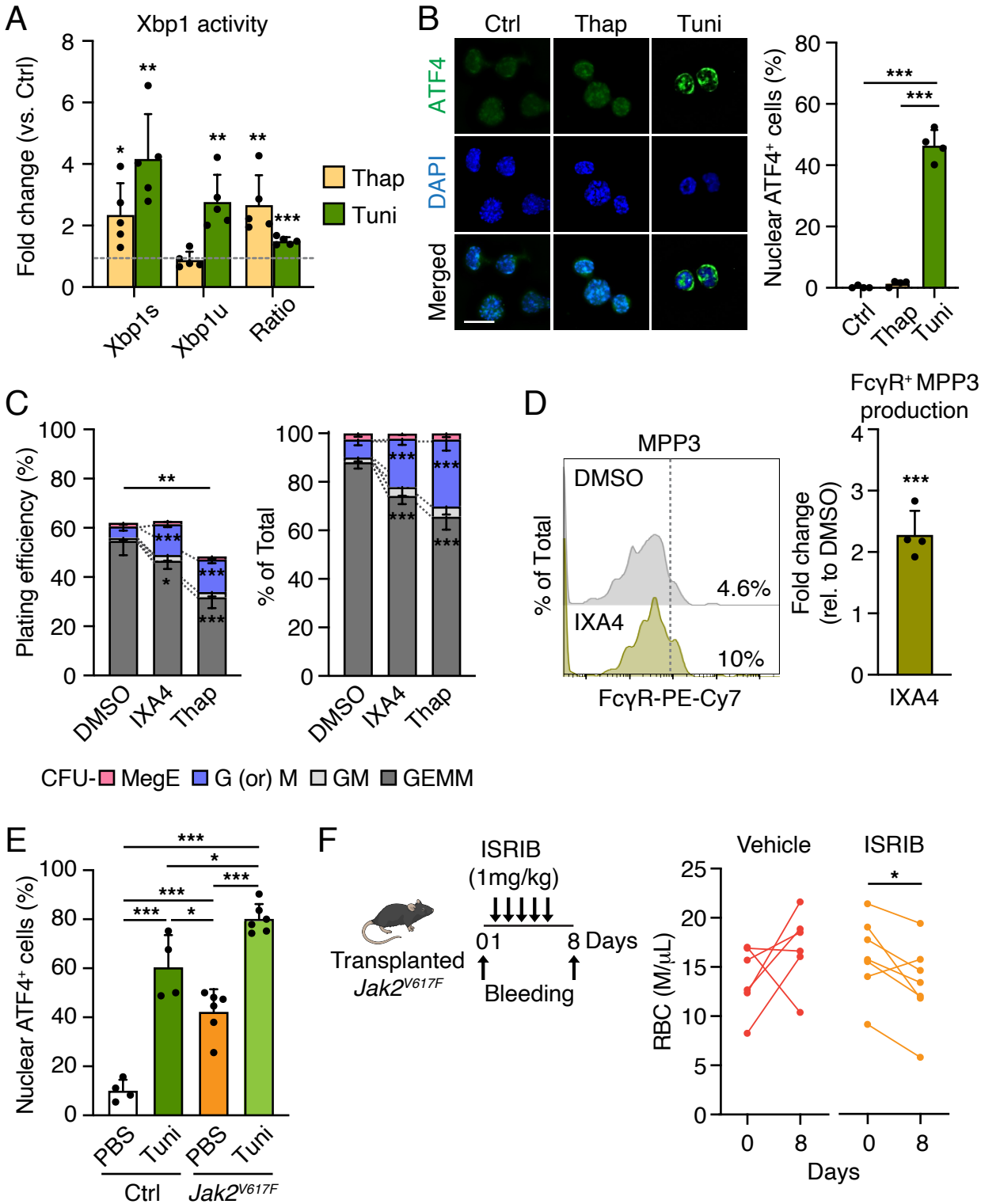
A
Xbp1 activity
Fold change (vs. Ctrl)
Thap
Tuni
Xbp1s
Xbp1u
Ratio
B
Ctrl
Thap
Tuni
ATF4
DAPI
Merged
Nuclear ATF4+ cells (%)
C
Plating efficiency (%)
% of Total
DMSO
IXA4
Thap
CFU- MegE G (or) M GM GEMM
D
MPP3
DMSO
IXA4
4.6%
10%
% of Total
FcγR-PE-Cy7
FcγR+ MPP3 production
Fold change (rel. to DMSO)
E
Nuclear ATF4+ cells (%)
PBS
Tuni
Ctrl
Jak2V617F
F
Transplanted Jak2V617F
ISRIB (1mg/kg)
0 1
8 Days
Bleeding
Vehicle
ISRIB
RBC (M/μL)
Days

Figure 4

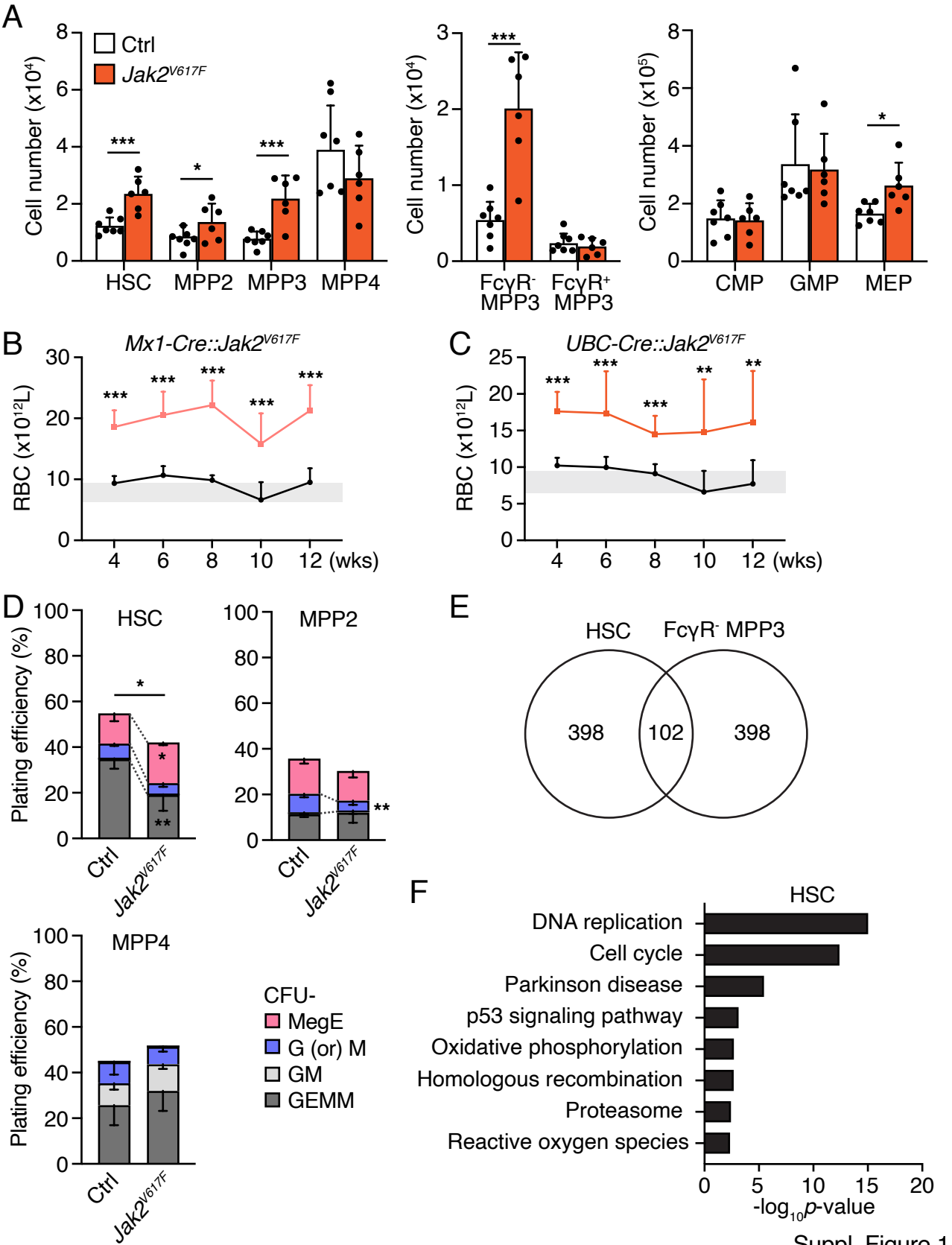

Suppl. Figure 1

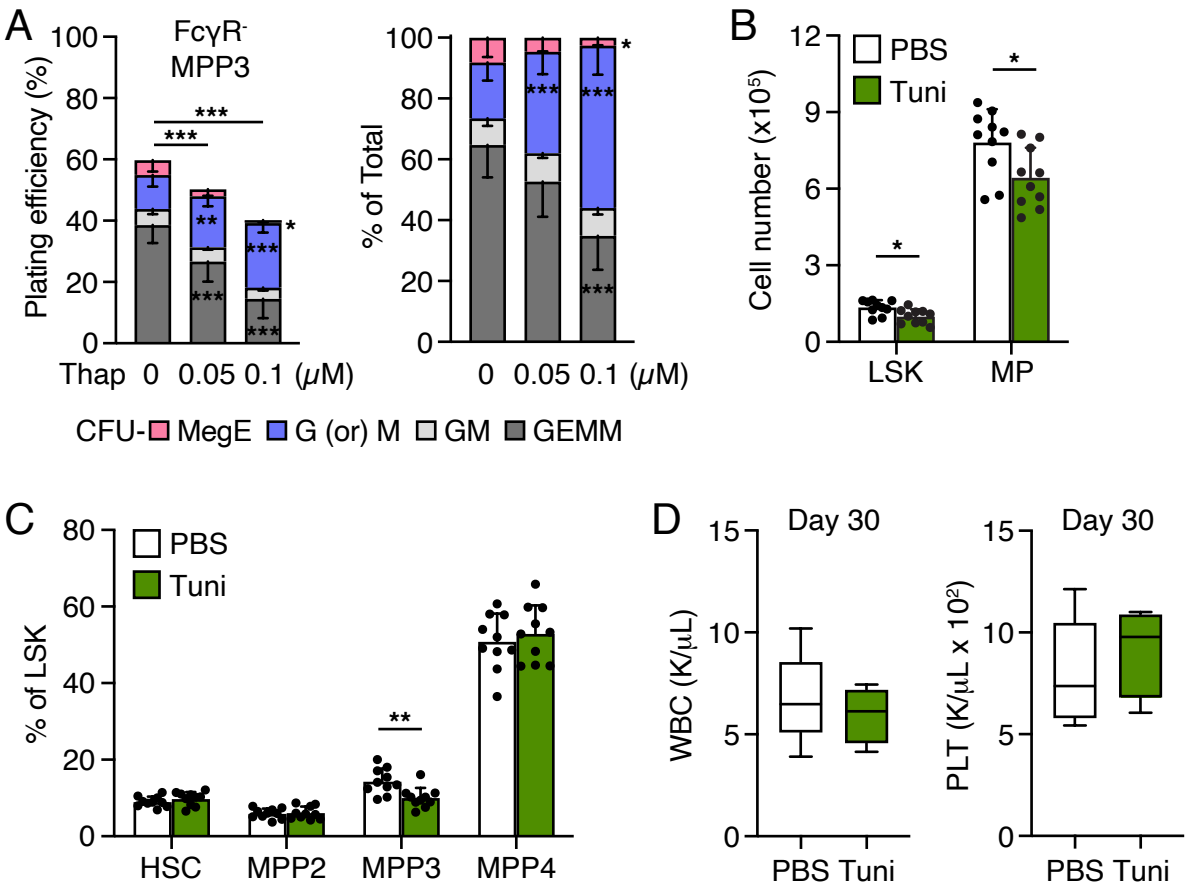

Suppl. Figure 2

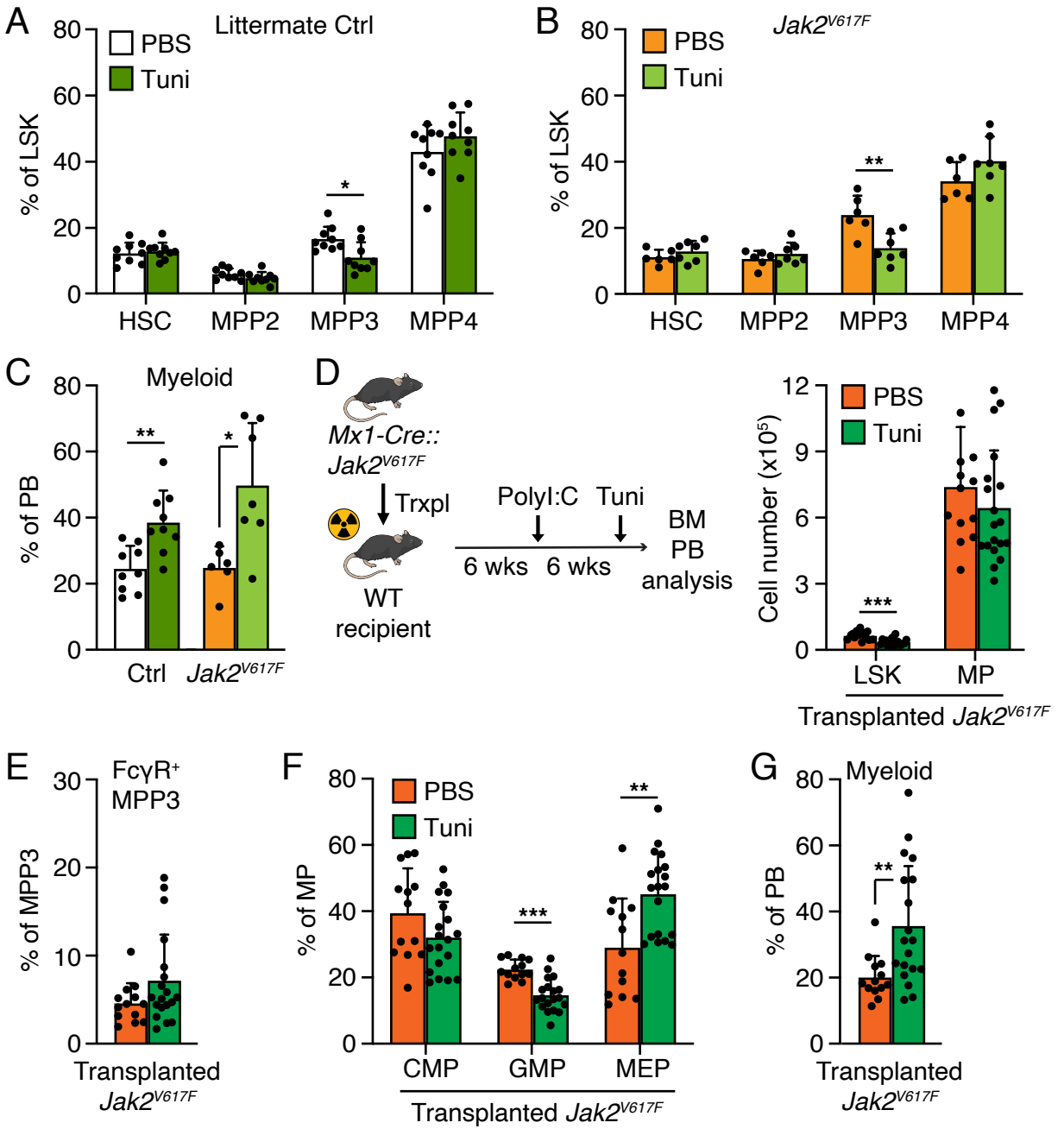

Suppl. Figure 3

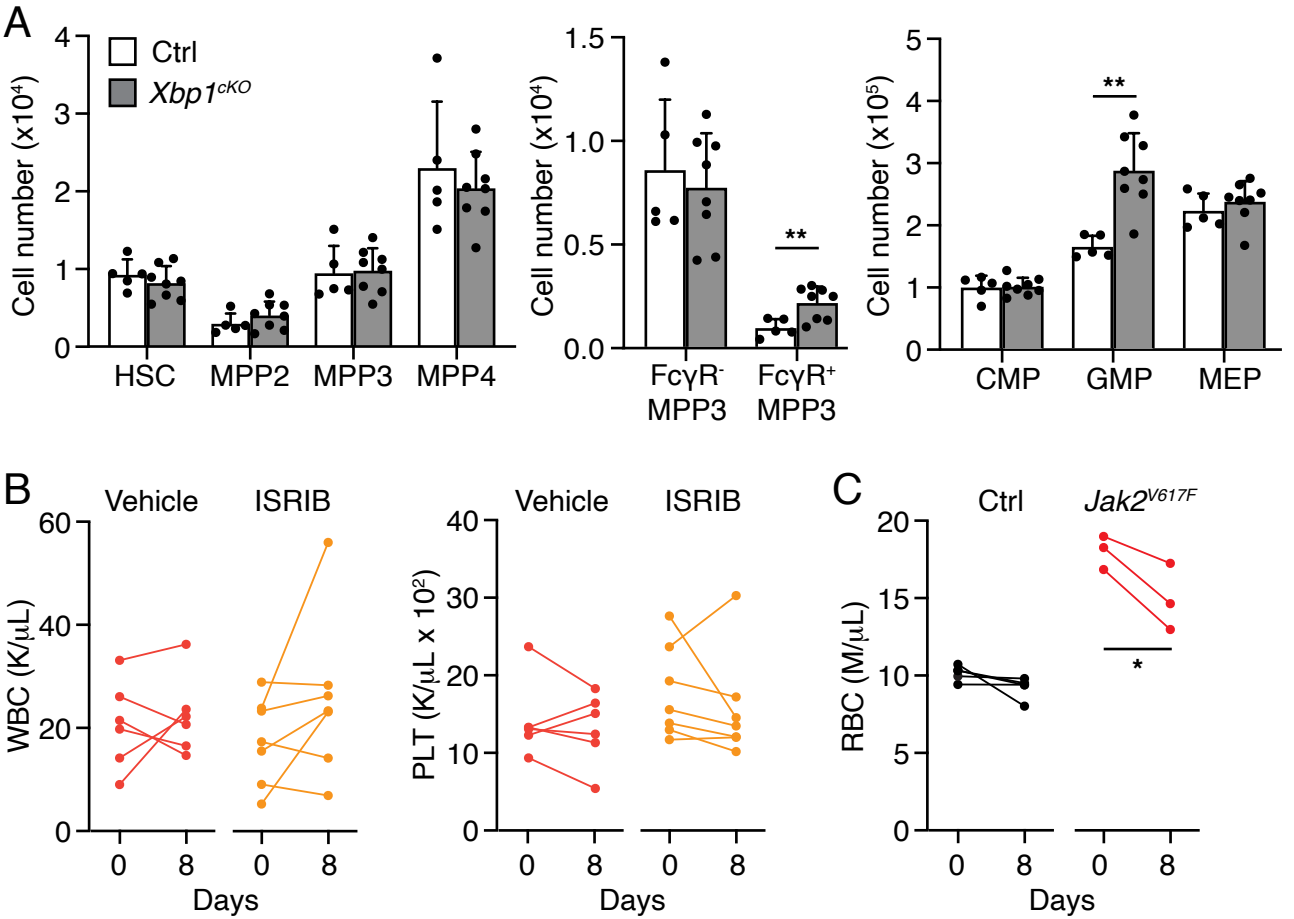

Suppl. Figure 4